Volume 206, Number 6, 15 December, 2011

ISSN 0257-8972

ELSEVIER

SURFACE & COATINGS TECHNOLOGY

Editors
H.C. Man
A. Matthews
J. Patscheider
I. Petrov

Available online at www.sciencedirect.com

SciVerse ScienceDirect

http://www.elsevier.com/locate/surfcoat

ScienceDirect

Keywords
Author name
Surface and Coatings Technology
Volume
Issue
Pages

Surface and Coatings Technology

SUPPORTS OPEN ACCESS

Volume 339

Pages 1-236 (15 April 2018)

Previous vol/issue | Next vol/issue

Show all article previews | Download PDFs | Export

Pages 155-166

Download PDF Article preview

Research article • Full text access

Influence of Ag additions on the structure, mechanical properties and oxidation behaviour of Cr-O coatings deposited by HiPIMS

F. Fernandes, T.B. Yaqub, A. Cavaleiro

Pages 167-180

Download PDF Article preview

Research article • Full text access

Three-dimensional numerical simulations of the particle loading effect on gas flow features for low pressure cold spray applications

F. Caruso, M.C. Meyer, R. Lupoi

Pages 181-190

Download PDF Article preview

Research article • Full text access

Influence of ball-burnishing on roughness, hardness and corrosion resistance of AISI 1045 steel

Alberto Saldaña-Robles, Héctor Plascencia-Mora, Eduardo Aguilera-Gómez, Adriana Saldaña-Robles, ... José Angel Diosdado-De la Peña

Pages 191-198

Download PDF Article preview

Research article • Full text access

The study of electrodeposition of hydroxyapatite-ZrO_2-TiO_2 nanocomposite coatings on 316 stainless steel

Morteza Poorraeisi, Abdollah Afshar

Pages 199-207

Download PDF Article preview

Research article • Full text access

Improving the surface characteristics of Ti-6Al-4V and Timetal 834 using PIRAC nitriding treatments

B. Attard, A. Leyland, A. Matthews, E.Y. Gutmanas, ... G. Cassar

Pages 208-223

Download PDF Article preview

Research article • Full text access

Cold spray additive manufacturing: A viable strategy to fabricate thick B_4C/Al composite coatings for neutron shielding applications

N.H. Tariq, L. Gyansah, J.Q. Wang, X. Qiu, ... T.Y. Xiong

Pages 224-236

Download PDF Article preview

ISSN: 0257-8972

Copyright © 2018 Elsevier B.V. All rights reserved

ELSEVIER About ScienceDirect Remote access Shopping cart Contact and support Terms and conditions Privacy policy

We use cookies to help provide and enhance our service and tailor content and ads. By continuing you agree to the use of cookies.

Copyright © 2018 Elsevier B.V. or its licensors or contributors. ScienceDirect ® is a registered trademark of Elsevier B.V.

RELX Group™

Surface & Coatings Technology 339 (2018) 191–198

Contents lists available at ScienceDirect

Surface & Coatings Technology

journal homepage: www.elsevier.com/locate/surfcoat

Influence of ball-burnishing on roughness, hardness and corrosion resistance of AISI 1045 steel

Alberto Saldaña-Robles[a], Héctor Plascencia-Mora[b], Eduardo Aguilera-Gómez[b], Adriana Saldaña-Robles[a], Alfredo Marquez-Herrera[a], José Angel Diosdado-De la Peña[b,*]

[a] Universidad de Guanajuato, Campus Irapuato-Salamanca, Departamento de Ingeniería Agrícola, Carretera Irapuato-Silao, km 9, 36500, Ex Hacienda "El Copal", Irapuato, Guanajuato, Mexico

[b] Universidad de Guanajuato, Campus Irapuato-Salamanca, Departamento de Ingeniería Mecánica, Carretera Salamanca-Valle de Santiago, km 3.5 + 1.8, 36885, Comunidad de Palo Alto, Salamanca, Guanajuato, Mexico

ARTICLE INFO

Keywords:
Ball-burnishing
Factorial design
Hardness
Surface roughness
Corrosion resistance

ABSTRACT

The ball-burnishing process involves a surface plastic deformation that improves the physical-mechanical properties of manufactured parts. In this work, was used to study the influence of the main parameters of the ball-burnishing process on features such as mean surface roughness and hardness of cylindrical AISI 1045 steel samples. The experimental stage was based on a 3^3 factorial design and the Response Surface Methodology. An equation was proposed to model the mean roughness in the studied experimental region. Moreover, the polarization technique (Tafel) and electrochemical impedance spectroscopy (EIS) were used to evaluate the burnishing process effect on corrosion resistance of a sample machined with the optimal burnishing parameters obtained herein. Finally, burnishing process effect on the phase change was also evaluated by using X-ray diffraction. As a result, the factor that showed higher influence was the burnishing force for both features, roughness and hardness. The data shows that it is possible to reduce the surface roughness from 3.51 μm to 0.61 μm and to increase the hardness from 202 HB to 236 HB using ball-burnishing process, and to improve the corrosion resistance in AISI-1045 steel.

1. Introduction

The ball-burnishing process creates a surface plastic deformation (SPD) that uses a ball with 3–20 mm diameter as deforming element [1]. The ball applies a normal force high enough to produce a plastic deformation on the surface which displaces the material from ridges to depressions on superficial micro-irregularities [2], Fig. 1. Burnishing is considered as a simple and low-cost process with advantages such as improving the physical and mechanical properties of the manufactured parts [3]; decreasing surface roughness [4–8], offering of good finishing accuracy, increasing hardness on the workpiece surface [6–9], inducing compressive residual stresses [9,10], which as consequence, improves wear resistance [11], fatigue [10] and corrosion [12]. These properties might help to extend the expected lifetime of the treated piece. Among other parameters, the mean roughness and the surface hardness is considered as the most important parameter in the measurement of surface integrity. According to the literature, the surface roughness, after being treated by the ball-burnishing process, can be improved between 40% and 90% [6,7,13]; while the hardness can be improved between 17% and 60% [6,14–16]. The percentage of improvement depends on the parameters used during the burnishing process as well as the material studied.

Currently, a variety of systematics approaches to specific parameters of ball-burnishing allows a deeper understanding on the process, with the purpose of being optimized [17,18]. The variables commonly proposed by the literature are burnishing force, feed and speed [19]. In various experimental studies a factorial design (DF) was used [15,20,21]; whereas in others, a different method, the Response Surface Methodology (MSR) [22,23] was satisfactory as an analysis method. Several authors agree that the burnishing force is a factor that improves the surface roughness, given that as the force increases, the roughness decreases [6,18,24] and the hardness increases [6,16,25]. Other authors agree that the force is the most influential parameter in the process [26,27], followed by the feed [26], whereas the speed parameter is not too significant; it is even considered as a negligible parameter in the process [6,26,27].

Another property that helps to substantially improve lifetime of the burnished component is the corrosion resistance. This property has

* Corresponding author.
E-mail addresses: alberto.saldana@ugto.mx (A. Saldaña-Robles), hplascencia@ugto.mx (H. Plascencia-Mora), eag@ugto.mx (E. Aguilera-Gómez), adriana.saldana@ugto.mx (A. Saldaña-Robles), amarquez@ugto.mx (A. Marquez-Herrera), jose.diosdado@ugto.mx (J.A. Diosdado-De la Peña).

https://doi.org/10.1016/j.surfcoat.2018.02.013
Received 25 August 2017; Received in revised form 11 January 2018; Accepted 3 February 2018
Available online 05 February 2018
0257-8972/ © 2018 Elsevier B.V. All rights reserved.

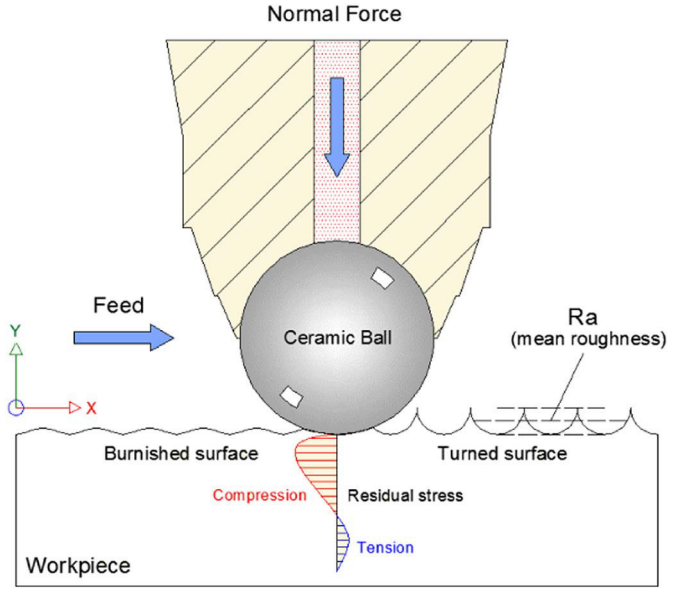

Fig. 1. Schematic of ball-burnishing process.

been mainly studied in aluminum alloys [28–30] and steels [31–35], subjected to different processes such as burnishing with a cylindrical-ended polycrystalline diamond (PCD) tool [28–30], ball-burnishing or low plasticity burnishing with a ball [31,32,35,36], dry roller-burnishing [33,34,37] and cryogenic burnishing with roller or ball [37–39]. In the literature, the effect of the burnishing process on the corrosion resistance was generally conducted by electrochemical impedance spectroscopy (EIS), Potentiodynamic Polarization, Galvanostatic Techniques, Potentiostatic Polarization or Mott–Schottky plots [28–39]. According to Al-Qawabeha et al. [33], the burnishing process can considerably increase the resistance corrosion because it produces a fine-grained surface zone in A53 steel using HCl solution. Pu et al. [38] attributed the mechanism of grain refinement to the dynamic recrystallization. Hryniewicz and Rokosz [34] and Jinlong et al. [29] showed a similar conclusion to Al-Qawabeha et al. [33], but on 2024 aluminum alloy and C45 carbon steel, respectively, both in NaCl solution. Jinlong et al. [28] found a better corrosion resistance of burnished samples of aluminum alloy with the higher burnishing force. Other studies showed that the corrosion resistance was improved on various materials by different types of burnishing due to grain refinement [35–39]. Nonetheless, the corrosion behavior of an AISI-1045 steel after ball-burnishing has not been reported yet in the literature.

In this work, a ball-burnishing tool with a mechanical spring was used for the experimental tests on cylindrical AISI 1045 steel samples. The experimental study followed a factorial design using the Response Surface Methodology, in which the influence of the most important parameters suggested by the literature was studied. Based on the statistical analysis, an equation to model the mean roughness was proposed and evaluated. Also, an optimal parameter set was obtained, and a sample was machined using this set. Subsequently, this sample was subjected to complementary corrosion and phase change tests. The following section details the samples sets and experimental procedure.

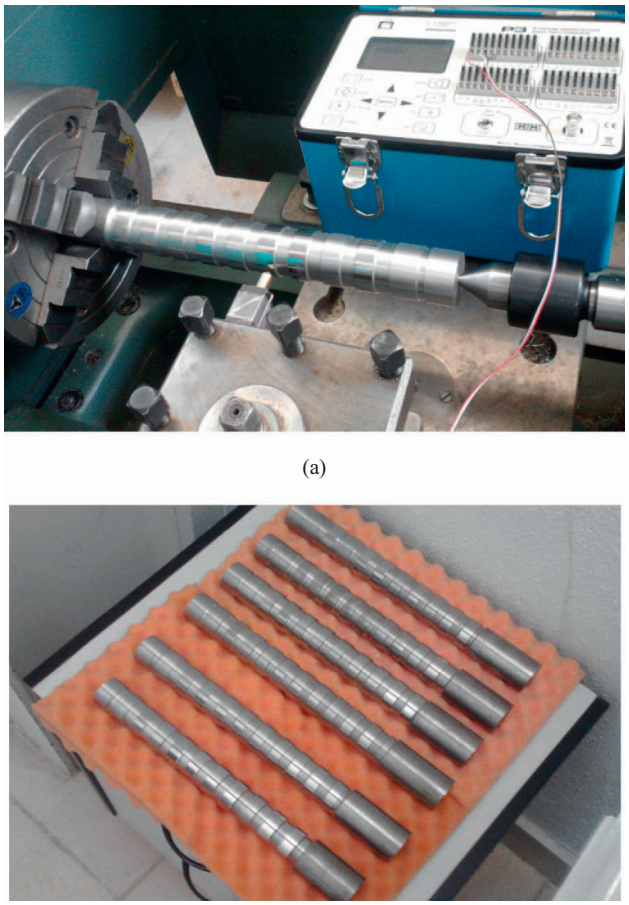

(a)

(b)

Fig. 3. Test sample; a) burnished sample; b) burnished set after 54 experimental samples.

2. Material and methodology

2.1. Workpiece material

AISI 1045 steel was used in this work, given that it is widely used in the automotive industry [6]. Its chemical composition was provided by the supplier and is shown in Table 2.

The test samples were cylindrical pieces with 10 divisions each. On these test samples, segments 1 through 9 were turned and burnished, while segment 10 was just turned. A scheme of the test sample with its intended characteristics is shown in Fig. 2. This test sample is similar to the test sample proposed by Brostow et al. [40].

Fig. 3(a) shows a test sample as it is being burnished, while Fig. 3(b) presents the six cylindrical samples before mean roughness and Brinell hardness measurements.

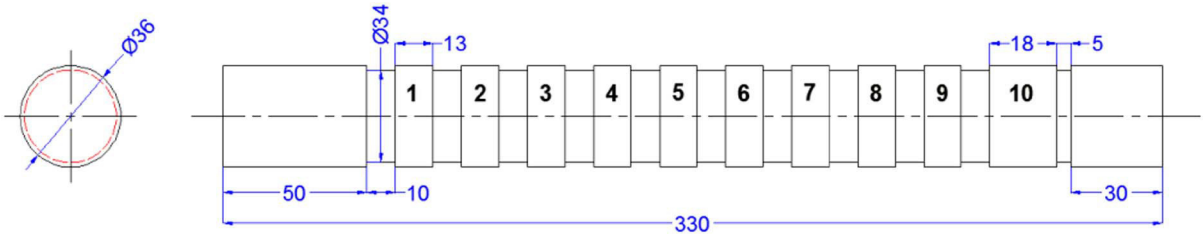

Fig. 2. Orthogonal views of the test sample; segments 1 through 9 were turned and burnished and segment 10 was just turned (mm).

Table 1
Burnishing experimental variables.

Level	Speed A ($m \cdot min^{-1}$)	Feed B ($mm \cdot rev^{-1}$)	Force C (N)
Low	35	0.2	98
Medium	53	0.4	196
High	71	0.6	294

2.2. Experimental study of burnished cylindrical samples

Firstly, 3^3 factorial design was used as statistical methodology, it was completely randomized with 2 replicas [41]. This statistical study is focused on the effect parameters such as speed (A), feed (B) and burnishing force (C) on the mean roughness (R_a) and Brinell hardness (HB) after a ball-burnishing process. The factorial experiment consisted of a total of 54 experimental sets, over the samples shown in Fig. 3(b). The samples were initially turned on a horizontal lathe TRENS® SN 32 (speed of 101.8 $m \cdot min^{-1}$ and feed of 0.1 $mm \cdot rev^{-1}$), and immediately burnished by using a diamond burnishing tool EDP# S2300-00 (12.7 mm ball diameter), with different conditions of burnishing force, speed and feed as listed in Table 1.

A profilometer Mitutoyo® model Surftest-211 was used to measure the mean roughness according to ISO 4287 standard [42], these measurements were made on the same direction as the burnishing process was applied. The Brinell hardness of each test region was measured by using a portable hardness tester Hardmatic® model HH-411. The data was analyzed by using the statistical software Statgraphics® Centurion XVI.

2.3. Corrosion evaluation

Secondly, a corrosion characterization was carried out on a sample prepared with the optimum parameters identified for best hardness conditions. To have an adequate comparison, also only-turned samples were characterized.

The corrosion resistance of the samples was tested using a VersaStart3-500 electrochemical interface from Princeton Applied Research Inc., which contained a frequency response analyzer (FRA). The corrosion study was conducted using the polarization technique (Tafel) and electrochemical impedance spectroscopy (EIS). Tafel and EIS were performed using 3.5 wt% NaCl solution in a conventional 3-electrode cell at room temperature. An Ag/AgCl (3.5 M KCl) electrode and a platinum mesh were used as the reference and counter electrode, respectively. An area of 0.5 cm^2 of steel substrate was used as the working electrode. Before the measurements, an open circuit potential (OCP) was applied for 30 min. For the impedance test, a sinusoidal AC signal of 10 mV (rms) amplitude and sweep from 100,000 Hz to 0.1 Hz were used. Tafel plots were obtained in a single scan beginning at −250 mV vs. corrosion potential, E_{corr} (cathodic Tafel plot) and scanning continuously to +250 mV vs. E_{corr} (anodic Tafel plot). A step of 1 mV every 2 s (0.5 mV/s) was used. The resulting curve is a plot of the applied potential vs. the logarithm of the measured current.

2.4. Phase change evaluation

Finally, X-ray diffraction (XRD) measurement was performed on the optimum parameters sample, with a Rigaku X'pert diffractometer using the $Co_{K\alpha}$ line ($k\alpha$ = 1.7903 Å).

Table 2
Chemical composition of AISI 1045 steel (%).

P	S	Sn	C	Cu	Mo	Si	Ni	Cr	Mn
0.01	0.02	0.01	0.48	0.16	0.02	0.22	0.10	0.11	0.64

Table 3
Factorial design matrix and experimental results.

Exp. number	Force F (N)	Feed A ($mm \cdot rev^{-1}$)	Speed V ($m \cdot min^{-1}$)	Roughness R_a (μm)	Hardness (HB)
1	98	0.2	35	1.91	221
2	98	0.2	53	2.01	220
3	98	0.2	71	2.37	219
4	98	0.4	35	2.64	222
5	98	0.4	53	2.61	219
6	98	0.4	71	2.76	219
7	98	0.6	35	2.88	220
8	98	0.6	53	2.76	222
9	98	0.6	71	3.13	218
10	196	0.2	35	1.12	231
11	196	0.2	53	1.66	225
12	196	0.2	71	1.05	227
13	196	0.4	35	2.02	225
14	196	0.4	53	1.96	225
15	196	0.4	71	1.88	225
16	196	0.6	35	2.47	225
17	196	0.6	53	2.32	226
18	196	0.6	71	2.68	224
19	294	0.2	35	0.73	235
20	294	0.2	53	0.89	233
21	294	0.2	71	0.68	236
22	294	0.4	35	1.55	234
23	294	0.4	53	1.51	236
24	294	0.4	71	1.44	236
25	294	0.6	35	1.96	235
26	294	0.6	53	1.89	235
27	294	0.6	71	2.27	228
28	98	0.2	35	2.12	222
29	98	0.2	53	2.34	221
30	98	0.2	71	2.00	223
31	98	0.4	35	2.83	219
32	98	0.4	53	2.68	219
33	98	0.4	71	2.97	220
34	98	0.6	35	3.08	218
35	98	0.6	53	2.99	219
36	98	0.6	71	3.25	219
37	196	0.2	35	1.14	228
38	196	0.2	53	1.26	225
39	196	0.2	71	1.28	226
40	196	0.4	35	1.76	225
41	196	0.4	53	1.62	225
42	196	0.4	71	1.77	225
43	196	0.6	35	2.38	227
44	196	0.6	53	2.53	225
45	196	0.6	71	2.61	224
46	294	0.2	35	0.71	233
47	294	0.2	53	0.91	234
48	294	0.2	71	0.61	235
49	294	0.4	35	1.27	232
50	294	0.4	53	1.53	234
51	294	0.4	71	1.56	235
52	294	0.6	35	2.03	234
53	294	0.6	53	2.16	233
54	294	0.6	71	1.81	235

3. Results

3.1. Effect of the main parameters on the mean roughness

The factorial study of the three main parameters (A, B and C) with three levels each (a, b and c), allows to investigate ten different effects: A, B, C, AB, AC, BC, ABC, A^2, B^2 and C^2. As a consequence, they can raise ten null hypotheses to be proved, such as: H_0: A = 0 (no significant effect of factor A "speed" on R_a), H_0: B = 0 (no significant effect of factor B "feed" on R_a), …, H_0: ABC effect = 0 (no interaction effect ABC's "speed, feed and force" above R_a). The results of the 54 experiments carried out in this study based on the factorial design are shown in Table 3.

Once the assumptions of normality for the average surface roughness were accomplished, the analysis of variance (ANOVA) for R_a is

Table 4
ANOVA for mean roughness.

VS	SS	DF	MS	F_0	p-Value
A:Speed	0.0642	1	0.0642	2.34	0.1333
B:Feed	11.5713	1	11.5713	422.11	0.0000
C:Force	13.2253	1	13.2253	482.45	0.0000
AA	0.0027	1	0.0027	0.10	0.7552
AB	0.0198	1	0.0198	0.72	0.3997
AC	0.0338	1	0.0338	1.23	0.2733
BB	0.0690	1	0.0690	2.52	0.1199
BC	0.2109	1	0.2109	7.69	0.0082
CC	0.3136	1	0.3136	11.44	0.0015
ABC	0.0016	1	0.0016	0.06	0.8102
Error	1.1788	43	0.0274		
Total	26.6911	53			

VS = variability source; SS = sum of squares; DF = degrees of freedom; MS = mean square; F_0 = test statistic; p-value = observed significance.

Table 5
Kruskal-Wallis analysis and LSD test for Brinell hardness.

Factor	Units	Level	K-W statistic	p-Value (K-W)	Medians LSD	(p < 0.05) LSD
Force (C)	N	98	47.4308	0.0000[a]	220.0 α	1.1344
		196			225.7 β	
		294			234.1 γ	
Feed (B)	mm·rev^{-1}	0.2	0.7443	0.6892	227.4 α	4.1099
		0.4		N.S.	226.4 α	
		0.6			225.9 α	
Speed (A)	m·min^{-1}	35	0.0643	0.9683	227.0 α	4.1278
		53		N.S.	226.4 α	
		71			226.3 α	

Note: α, β and γ indicate statistical groups; N.S. these values indicate no significant difference.
[a] Indicates significant difference.

Table 6
Parameters of the proposed equivalent circuit.

Parameters[a]	Turning	Burnishing
Resistance, Ω cm^{-2} (R_{sol})	25.23	18.94
CPE, Yo, S-sec^n (Q)	74.23×10^{-6}	50.21×10^{-6}
$0 < n < 1$	70.81×10^{-2}	54.32×10^{-3}
Resistance, Ω cm^{-2} (R)	2537	15,690

[a] With measurement and fitting errors lower than 5%.

presented in Table 4. According to the analysis of data, it can be concluded that the main factors such as the force (C) and feed (B), the interaction force-feed (BC) and the quadratic effect of the force (C^2) have a significant effect on R_a with a 95% confidence level.

Thus, these effects are plotted on a Pareto chart, as shown in Fig. 4(a). Here, it can be observed that the burnishing force has the greatest effect on R_a, followed by the feed, the quadratic effect of the force and the force-feed interaction. From the analysis of the sum of squares (SS) in the Table 4, it was concluded that the burnishing force and feed are the principal parameters affecting the mean roughness; their contribution of percentage on the mean roughness were 43.4% and 49.5%, respectively.

Fig. 4(b) shows the main effects on R_a. It can be seen that within the speed range studied (35 m·min^{-1}–71 m·min^{-1}), the speed shows no significant effect on R_a. In contrast, feed at its lowest value (0.2 mm·rev^{-1}) and burnishing force at its highest value (294 N) have a significant effect on R_a, reducing roughness from 3.51 μm to 0.61 μm. In the experimental range studied, it was observed that reducing the feed and increasing the force resulted in an improvement of R_a around 83%.

Later, a regression model was applied to the reduced data to model the R_a as function of the input parameters such as burnishing force (X_1), feed (X_2) and speed (X_3).

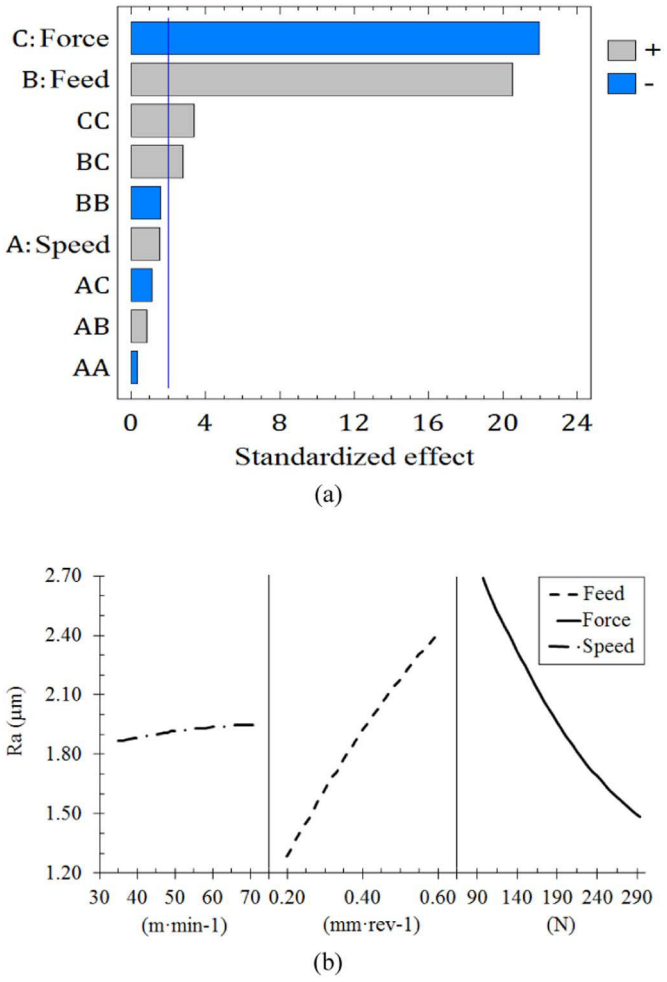

Fig. 4. a) Pareto chart for R_a, significance of effects upon ball-burnishing process; (b) Plot of main effects on R_a.

The adjusted multivariable regression model which describes the behavior of the roughness is represented in Eq. (1). This expression is only applicable under the specific conditions considered in this study. The magnitudes of the variables are specified in their original units.

$$R_a' = 2.413 - 1.357 \times 10^{-2}X_1 + 2.991X_2 + 8.225 \times 10^{-3}X_3 + 1.683 \times 10^{-5}X_1^2 - 1.896X_2^2 - 4.630 \times 10^{-5}X_3^2 + 4.783 \times 10^{-3}X_1X_2 - 2.126 \times 10^{-5}X_1X_3 + 7.986 \times 10^{-2}X_2X_3 \quad (1)$$

Fig. 5(a) shows the behavior of the mean roughness (R_a) on the experimental region and it is observed that increasing the burnishing force and decreasing the feed, resulted in a decrease of the mean roughness. Thus, it might be established that the optimum value of the mean roughness is around 0.61 μm, which was obtained with the parameters values: force of 294 N, speed of 71 m·min^{-1} and feed of 0.2 mm·rev^{-1}. The correlation coefficient (R^2) is considered a measure of the model's overall performance, indicating how well the data fits a statistical model. The results for R_a presented in the ANOVA, showed that the experimental data fit the model reasonably well with R^2 around 96%. This indicates that the burnishing force, feed and velocity explain about 96% of variance in the steel surface roughness.

To validate the model, one sample with three iterations was selected and subjected to the following ball-burnishing conditions: burnishing force of 147 N, feed of 0.3 mm·rev^{-1} and speed of 53 m·min^{-1}, which the mean R_a resulted in 2.16 μm on the surface steel. Whereas the R_a'

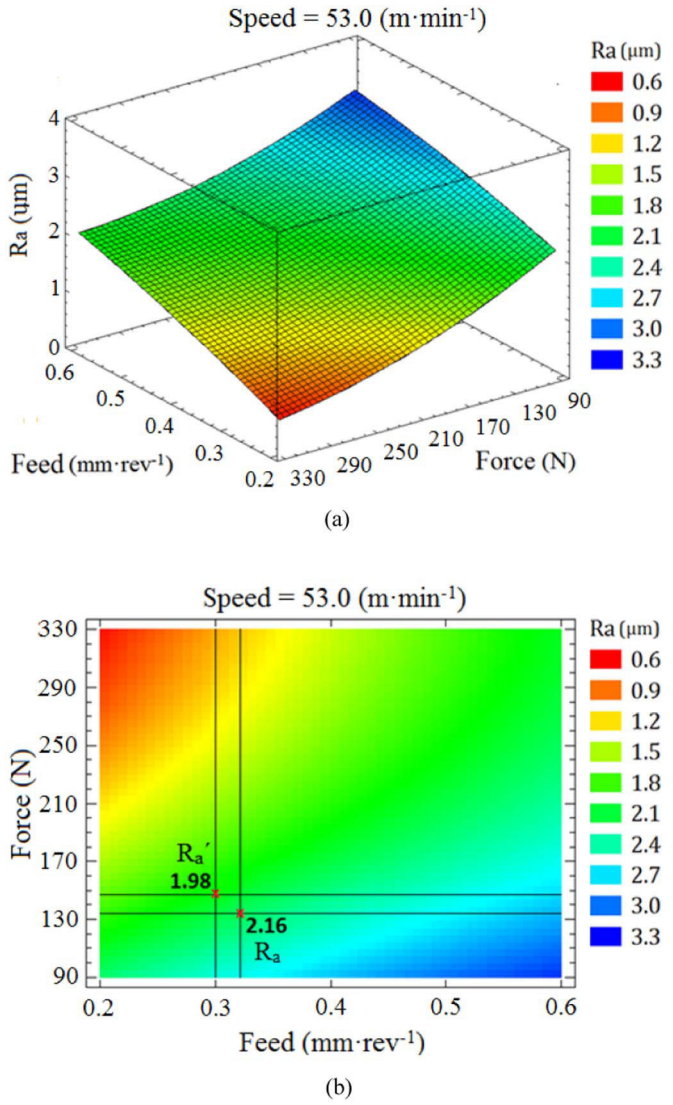

Fig. 5. a) Estimated response surface for mean roughness; b) contours of estimated response surface, R_a for experimental mean, R_a' for model value.

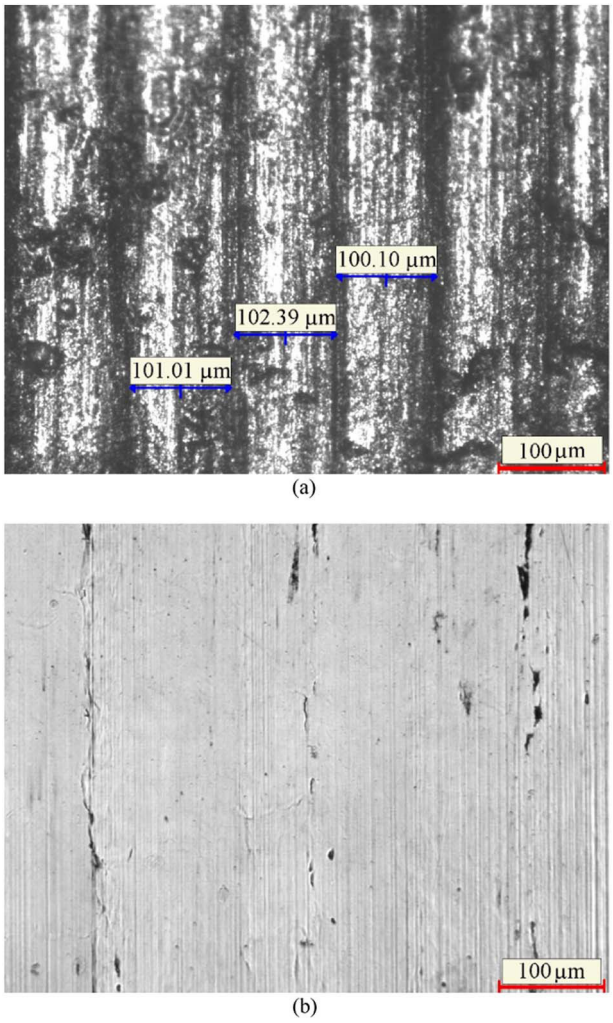

Fig. 6. Surface topography after: a) turning (100× magnification); b) optimal burnishing (100× magnification). Images obtained with Clemex L-Type High Definition Camera.

value in the model was around 1.98 µm, with an error of 8%, which implies adequacy of the model, see Fig. 5(b).

Fig. 6(a) shows the original surface after turning, where it is possible to see the marks of the turning feed (0.1 mm·rev^{-1}). In Fig. 6(b) the resultant surface after machining with the optimal burnishing conditions (force of 294 N, speed of 71 m·min^{-1} and feed of 0.2 mm·rev^{-1}) is observed.

3.2. Effect of the main parameters on the Brinell hardness

Since the data obtained for the response variable HB did not accomplish the assumptions of normality and a transformation did not correct the fitting, a non-parametric method of analysis was used [43]. The Kruskal-Wallis test (KW), which is the nonparametric alternative for the F-test of completely randomized design, was chosen. Additionally, the multiple comparison of means allocated ranges (median) treatment test, called Least Significant Difference (LSD) with $p < 0.05$ was used. The summary of the results of KW test is shown in Table 5, where it is pointed out that the force shows a rather significant difference for Brinell hardness, whereas the feed and speed show no statistical differences for this response variable at a confidence level of 95%.

The LSD test is also shown in Table 5, which indicates that the median values of Brinell hardness for feed and speed are very similar, and they belong to the same statistical group. For the burnishing force, it is shown that the medians belong to different statistical groups, proving that an increased surface hardness was obtained with a force of 294 N.

The ball-burnishing caused an improvement in the surface hardness on the burnished regions of the cylindrical samples of up to 14%, from 202 HB to 236 HB.

3.3. Effects of burnishing process on the corrosion resistance

The polarization curves (Tafel) and Nyquist diagrams (EIS) [44] were used to evaluate the effect of burnishing process on the corrosion resistance of an optimal burnished sample (burnishing force of 294 N and feed of 0.2 mm·rev^{-1}) and compared with a turned-only sample.

Fig. 7 shows the Tafel curves of burnished and turned samples. The values of corrosion potential (E_{corr}) and corrosion current (I_{corr}) were obtained from the polarization curves by the Tafel extrapolation method with fitting errors lower than 5%. The corrosion potential value for the turned sample, however, reached a higher value (Ec = −271.8 mV) in comparison to the burnished one (Ec = −293.4 mV). The average corrosion current value for surface after turning was 13.99 µA·cm^{-2}. Although the average corrosion potentials values obtained for samples after burnishing proved a slight increase in the susceptibility to corrosion, burnishing caused an important decrement of current value to 1.15 µA·cm^{-2}. This difference

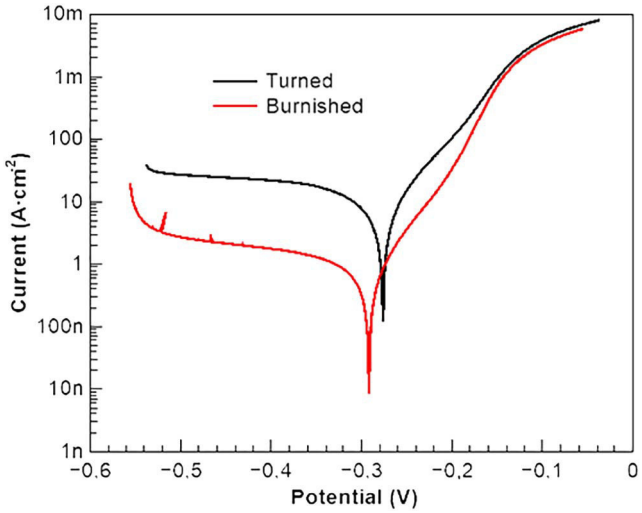

Fig. 7. Tafel curves of burnished and turned steel.

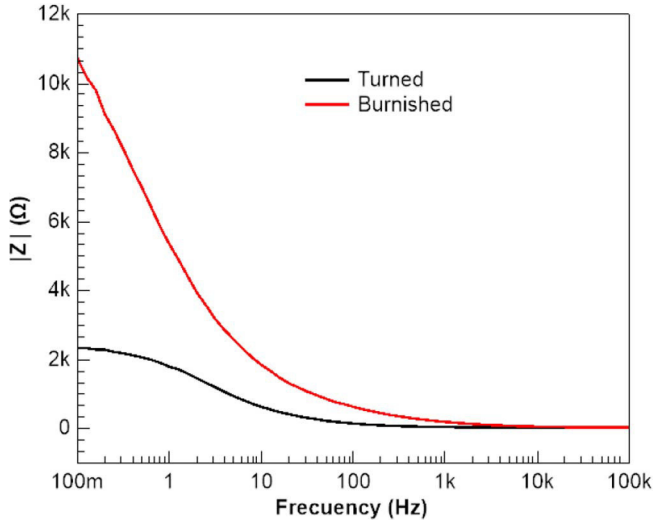

Fig. 9. Bode plots of turned and burnished sample.

suggests that the burnishing surface is more resistant to corrosion, since the charge-transfer on the turned sample is up to 12 time higher than on the burnished sample, therefore it effectively protects the surface of the corrosion. Also, Fig. 7 shows that the charge exchange activity at the interface for the burnished sample is lower than that of the turned sample, consequently, this decrease in the corrosion current, I_{corr}, infers that the burnished layers is more resistant to corrosion and it effectively protects the surface against the attack of the Cl- ions, which are responsible for the corrosion of steel.

The curves of electrochemical impedance spectroscopy (EIS) are shown in Fig. 8. These were obtained by testing the burnished and turned samples in NaCl aqueous solution. The inset in Fig. 8 shows the improved equivalent electrical circuit found for both samples. This circuit models the chemical behavior of the steel surface in the presence of chloride ions. In the case of the turned sample, R_{sol} is the solution resistance and R–Q may be the resistance and constant phase element of the turned steel substrate. For the burnished sample, in the equivalent circuit, R_{sol} is also the solution resistance, while Q represents the constant phase element and describes an imperfect behavior of a reactance; and the resistor, R, corresponds to the burnished layer.

Data fitted using equivalent electrical circuits are presented in Table 6, including the R_{sol}, Q, n and R values of the samples, with measurement errors lower than 5%. It has been established that high values of R imply a better corrosion protection capability on the surface. When $n = 1$, 0, 0.5 or $0.5 < n < 1$, Q represents a capacitor, resistor, uniform diffusion or a rough electrode, respectively [45].

The Bode plots are shown in Fig. 9. The absolute values of the impedance are plotted on the Y-axis with log frequency on the X-axis. The main effect of burnishing process is an increase in the impedance modulus, |Z|, with frequencies below 1 kHz, as well as an increase in polarization resistance, R. These results also suggest that turned sample is less resistant to corrosion than burnished one.

Likewise, Table 6 shows that the higher charge-transfer resistance was developed by the burnished sample with 15,690 Ω·cm^{-2}. Here, it must be emphasized that the result of the resistance, R, is inversely proportional to the corrosion rate, where a high R corresponds to a low rate of corrosion. It is noted that for both samples, R_{sol} is very similar as expected since the same solution was used. Additionally, the literature suggest that the charge-transfer resistance is related with the diameter of the capacitive arc at the high frequency region, therefore a larger diameter of the capacitive arc indicates a better corrosion resistance for magnesium alloys after burnishing [32,37,38]. Hence, Fig. 8 also shows that the burnished AISI-1045 steel sample had a larger diameter of the capacitive arc than the only-turned sample, which corroborates that the burnished sample improved its corrosion resistance.

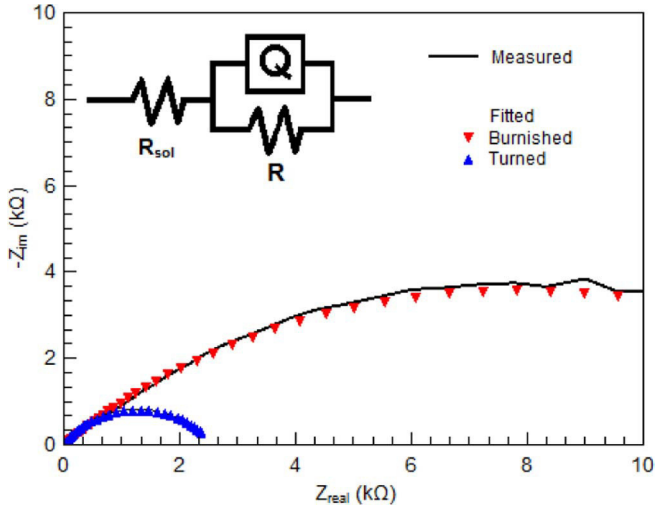

Fig. 8. Simulated spectrums and theirs experimentally generated impedance diagrams for the burnished and turned samples in NaCl 3.5wt% solution. The inset corresponds to the proposed model for the equivalent circuit on steel sample.

3.4. Effects of burnishing process on the phase

Fig. 10 shows the XRD patterns of optimal burnished and turned samples. All the XRD patterns exhibit two prominent peaks at various scattering angles, which are assigned to the (101) and (200) crystal planes (Card 96-900-6604), respectively [46].

Apparently, there are no distinct phase changes and the surface remains a cubic type structure (space group 1m-3m) as a function of surface treatment. The magnified view of the (101) and (200) peaks of sample for burnished and turned sample are shown in Fig. 11(a) and (b).

All the peaks exhibit significant shift to lower angles when sample is burnishing, indicating lattice expansion of surface material, as can be calculated from Eqs. (2) and (3).

From the Bragg law,

$$d = n\lambda/2\sin\theta \tag{2}$$

For the cubic system,

$$a = d\sqrt{h^2 + k^2 + l^2} \tag{3}$$

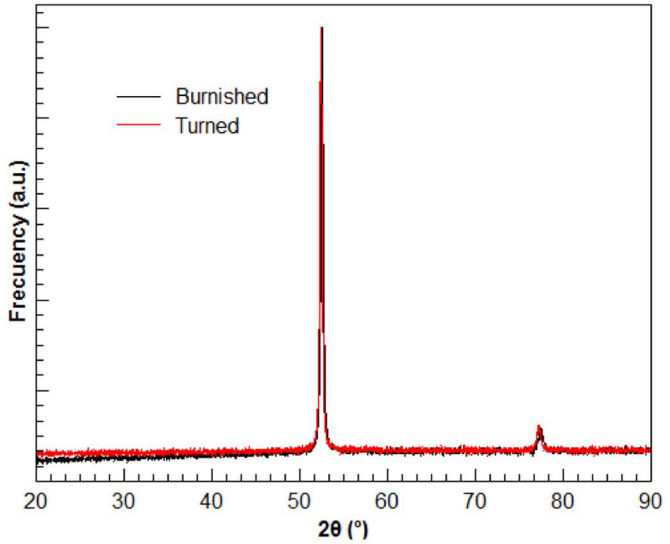

Fig. 10. The XRD patterns of burnished and turned sample.

where λ is wavelength of incident radiation, d is the lattice spacing, θ is the diffraction angle, a is the lattice parameter, and h, k, l are the Miller index of the crystal plane.

The lattice parameter of samples was calculated by means of the Rietveld method and Fullprof Suite software [47]. The crystal data of each phase used in the quantitative phase analysis were obtained from Crystallography Open Database (COD) [46].

From the literature review, improvement on the corrosion resistance is attributed to the grain refinement generated by the burnishing process. Herein, the result shows that the lattice parameter increases from 2.8604×10^{-10} m to 2.8693×10^{-10} m with an adjust factor $R_{WP} < 3\%$, suggesting d-spacing increases with burnishing. This change can explain the changes in mechanic properties, however further study is needed.

4. Conclusions

An improvement in the mean roughness and surface hardness was obtained through the process of ball-burnishing on cylindrical bars of commercial AISI 1045 steel. The mean roughness indicator showed an improvement in the surface quality of around 83%. The surface hardness showed an improvement around 14%, from 202 HB to 236 HB.

In the experimental study region, a maximum reduction of R_a from 3.51 μm to 0.61 μm was achieved by using a burnishing force of 294 N, feed of 0.2 mm·rev^{-1} and speed of 71 m·min^{-1}. The statistical analysis showed that the speed is not a significant factor for R_a; whereas, force and feed are significant. Also, it was observed that a reduction in the feed with an increase of force results in an improvement of the surface quality. The statistical analysis showed that only the burnishing force was found as an essential parameter for increasing the surface hardness.

An equation to model the mean roughness in the experimental region was proposed with a correlation coefficient of around 96% and it can be used to reduce experimental tests to obtain a specified mean roughness, with a maximum error of 8%.

A charge-transfer decrement along with a high resistance on the optimal burnished sample leads to a conclusion that burnishing process causes an increase of corrosion resistance, when compared with the turned sample.

A future work requires further experimental studies through X-ray diffraction and numerical simulations by using numerical analysis, such as FEM to find another response of interest, such as the compressive residual stresses on AISI 1045 steel.

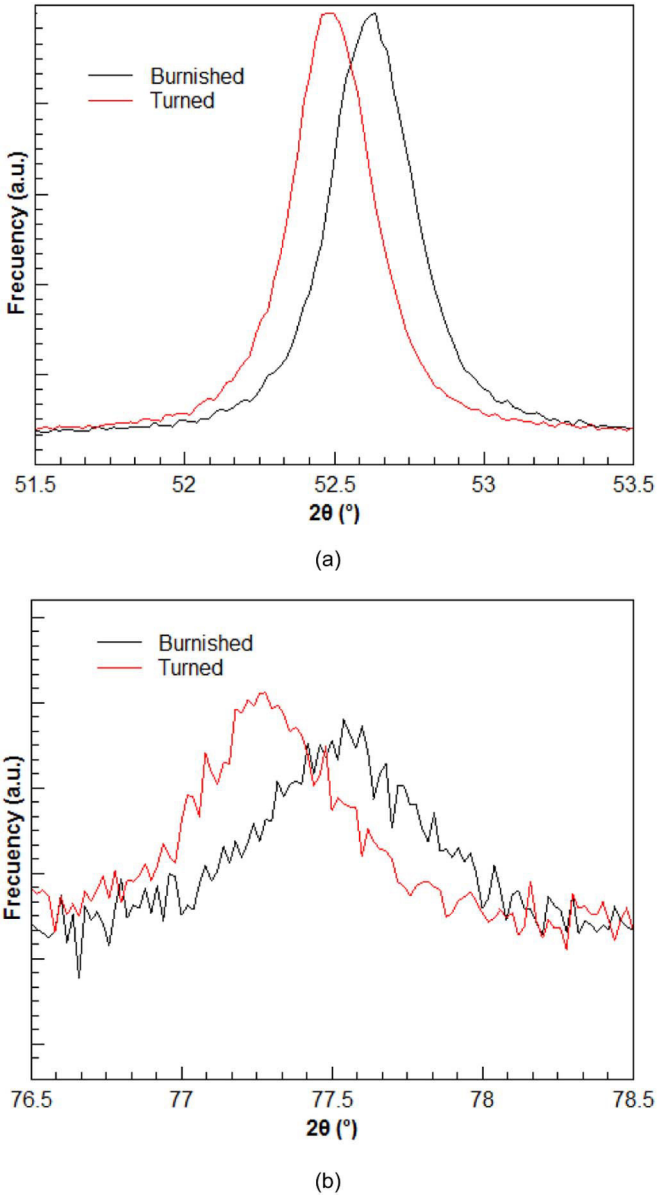

Fig. 11. Magnified view of the peaks of samples (a) (101) and (b) (200).

Acknowledgment

The authors would like to express their gratitude to the Departamento de Ingeniería Mecánica of the Universidad de Guanajuato for the equipment and material contributions during the development of this work. Also A. L. Saldaña-Robles acknowledges the financial support provided by the National Council for Science and Technology (CONACYT) during his doctoral studies.

References

[1] A. Saldaña-Robles, J.A. Diosdado-De la Peña, A.D.J. Balvantín-García, E. Aguilera-Gómez, H. Plascencia-Mora, N. Saldaña-Robles, El proceso de bruñido con bola: estado del arte de una tecnología en desarrollo, DYNA 92 (2017) 28–33, http://dx.doi.org/10.6036/7916.

[2] A. Saldaña-Robles, E. Aguilera-Gómez, H. Plascencia-Mora, E.R. Ledesma-Orozco, V.A. Alcántar, Análisis teórico-numérico de esfuerzos generados para bruñido de bola sobre cilindros rotativos, 20th Int. Conf. Mech. Eng., Santiago de Querétaro, México, 2014.

[3] J.A. Travieso, Estudio para la mejora del acabado superficial de superficies complejas, aplicando un proceso de deformación plástica, Universidad Politécnica de Cataluña, Bruñido con Bola, 2010.

[4] A.M. Hassan, A.M. Maqableh, The effects of initial burnishing parameters on non-

ferrous components, J. Mater. Process. Technol. 102 (2000) 115–121, http://dx.doi.org/10.1016/S0924-0136(00)00464-7.
[5] A. Bougharriou, K. Saï, W. Bouzid, Finite element modelling of burnishing process, Mater. Technol. 25 (2010) 56–62, http://dx.doi.org/10.1179/175355509X387110.
[6] A. Rodríguez, L.N. López de Lacalle, A. Celaya, A. Lamikiz, J. Albizuri, Surface improvement of shafts by the deep ball-burnishing technique, Surf. Coat. Technol. 206 (2012) 2817–2824, http://dx.doi.org/10.1016/j.surfcoat.2011.11.045.
[7] N.S.M. El-Tayeb, K.O. Low, P.V. Brevern, Influence of roller burnishing contact width and burnishing orientation on surface quality and tribological behaviour of aluminium 6061, J. Mater. Process. Technol. 186 (2007) 272–278, http://dx.doi.org/10.1016/j.jmatprotec.2006.12.044.
[8] H. Hamadache, L. Laouar, N.E. Zeghib, K. Chaoui, Characteristics of Rb40 steel superficial layer under ball and roller burnishing, J. Mater. Process. Technol. 180 (2006) 130–136, http://dx.doi.org/10.1016/j.jmatprotec.2006.05.013.
[9] Y.C. Yen, P. Sartkulvanich, T. Altan, Finite element modeling of roller burnishing process, CIRP Ann. Manuf. Technol. 54 (2005) 237–240, http://dx.doi.org/10.1016/S0007-8506(07)60092-4.
[10] F. Klocke, V. Bäcker, H. Wegner, M. Zimmermann, FE-analysis of the roller burnishing process for fatigue resistance increase of engine components, Engineering 225 (2011) 1–11, http://dx.doi.org/10.1243/09544054JEM2044.
[11] A.M. Hassan, S.Z.S. Al-Dhifi, Improvement in the wear resistance of brass components by the ball burnishing process, J. Mater. Process. Technol. 96 (1999) 73–80, http://dx.doi.org/10.1016/S0924-0136(99)00254-X.
[12] R.S. Díaz, N.T. Robert, C.O. Boada, Los tratamientos mecánicos superficiales para el acabado de las piezas, 5th Int. Conf. Mech. Eng., Santa Clara, Cuba, 2008.
[13] L.N. López De Lacalle, A. Lamikiz, J. Muñoa, J.A. Sánchez, Quality improvement of ball-end milled sculptured surfaces by ball burnishing, Int. J. Mach. Tools Manuf. 45 (2005) 1659–1668, http://dx.doi.org/10.1016/j.ijmachtools.2005.03.007.
[14] A.M. Hassan, A.S. Al-Bsharat, Influence of burnishing process on surface roughness, hardness, and microstructure of some non-ferrous metals, Wear 199 (1996) 1–8, http://dx.doi.org/10.1016/0043-1648(95)06847-3.
[15] D.S. Rao, H.S. Hebbar, M. Komaraiah, U.N. Kempaiah, Studies on the effect of ball burnishing parameters on surface hardness of HSLA dual-phase steels using factorial design, Trans. Indian Inst. Metals 61 (2008) 187–191, http://dx.doi.org/10.1007/s12666-008-0014-5.
[16] G.D. Revankar, R. Shetty, S.S. Rao, V.N. Gaitonde, Analysis of surface roughness and hardness in ball burnishing of titanium alloy, Measurement 58 (2014) 256–268, http://dx.doi.org/10.1016/j.measurement.2014.08.043.
[17] M.R. Stalin John, B.K. Vinayagam, Optimization of nonlinear characteristics of ball burnishing process using Sugeno fuzzy neural system, J. Braz. Soc. Mech. Sci. Eng. 36 (2014) 101–109, http://dx.doi.org/10.1007/s40430-013-0060-8.
[18] H. Hamadache, Z. Zemouri, L. Laouar, S. Dominiak, Improvement of surface conditions of 36CrNiMo6 steel by ball burnishing process, J. Mech. Sci. Technol. 28 (2014) 1491–1498, http://dx.doi.org/10.1007/s12206-014-0135-1.
[19] D. Mahajan, R. Tajane, A review on ball burnishing process, Int. J. Sci. Res. Publ. 3 (2013) 1–8.
[20] U.M. Shirsat, B.B. Ahuja, Parametric analysis of combined turning and ball burnishing process, Indian J. Eng. Mater. Sci. 11 (2004) 391–396.
[21] L. Luca, S. Neagu-Ventzel, I. Marinescu, Effects of working parameters on surface finish in ball-burnishing of hardened steels, Precis. Eng. 29 (2005) 253–256, http://dx.doi.org/10.1016/j.precisioneng.2004.02.002.
[22] A.M. Hassan, H.F.F. Al-Jalil, A.A. Ebied, Burnishing force and number of ball passes for the optimum surface finish of brass components, J. Mater. Process. Technol. 83 (1998) 176–179, http://dx.doi.org/10.1016/S0924-0136(98)00058-2.
[23] A. Sagbas, Analysis and optimization of surface roughness in the ball burnishing process using response surface methodology and desirabilty function, Adv. Eng. Softw. 42 (2011) 992–998, http://dx.doi.org/10.1016/j.advengsoft.2011.05.021.
[24] P. Babu, K. Ankamma, T. Prasad, A.V.S. Raju, N. Prasad, Optimization of burnishing parameters and determination of select surface characteristics in engineering materials, Sadhana 37 (2012) 503–520, http://dx.doi.org/10.1007/s12046-012-0092-2.
[25] F. Gharbi, S. Sghaier, K.J. Al-Fadhalah, T. Benameur, Effect of ball burnishing process on the surface quality and microstructure properties of AISI 1010 steel plates, J. Mater. Eng. Perform. 20 (2011) 903–910, http://dx.doi.org/10.1007/s11665-010-9701-6.
[26] T.A. El-Taweel, M.H. El-Axir, Analysis and optimization of the ball burnishing process through the Taguchi technique, Int. J. Adv. Manuf. Technol. 41 (2009) 301–310, http://dx.doi.org/10.1007/s00170-008-1485-6.
[27] U. Esme, Use of grey based Taguchi method in ball burnishing process for the optimization of surface roughness and microhardness of AA 7075 aluminum alloy, Mater. Technol. 44 (3) (2010) 129–135.
[28] L. Jinlong, L. Hongyun, X. Jinpeng, Experimental study of corrosion behavior for burnished aluminum alloy by EWF, EBSD, EIS and Raman spectra, Appl. Surf. Sci. 273 (2013) 192–198, http://dx.doi.org/10.1016/j.apsusc.2013.02.012.
[29] L. Jinlong, L. Hongyun, L. Tongxiang, Investigation of microstructure and corrosion behavior of burnished aluminum alloy by TEM, EWF, XPS and EIS techniques, Mater. Res. Bull. 83 (2016) 148–154, http://dx.doi.org/10.1016/j.materresbull.2016.05.013.
[30] L. Jinlong, L. Hongyun, Effect of surface burnishing on texture and corrosion behavior of 2024 aluminum alloy, Surf. Coat. Technol. 235 (2013) 513–520, http://dx.doi.org/10.1016/j.surfcoat.2013.07.071.
[31] K. Pałka, A. Weroński, K. Zaleski, Mechanical properties and corrosion resistance of burnished X5CrNi 18-9 stainless steel, J. Achiev. Mater. Manuf. Eng. 16 (2006) 57–62.
[32] P. Zhang, Z. Liu, Enhancing surface integrity and corrosion resistance of laser cladded Cr–Ni alloys by hard turning and low plasticity burnishing, Appl. Surf. Sci. 409 (2017) 169–178, http://dx.doi.org/10.1016/j.apsusc.2017.03.028.
[33] U. Al-Qawabeha, A.E. Al-Rawajfeh, E. Al-Shamaileh, Influence of roller burnishing on surface properties and corrosion resistance in steel, Anti-Corros. Methods Mater. 56 (2009) 261–265, http://dx.doi.org/10.1108/00035590910989552.
[34] T. Hryniewicz, K. Rokosz, Corrosion behaviour of C45 Carbon steel after roller burnishing, 23rd Int. Conf. Metall. Mater. Met., Brno, Czech Republic, 2014 http://metal2014.tanger.cz/files/proceedings/metal_05/papers/77.pdf.
[35] W.B. Saï, O. Tsoumarev, E. Triki, Influence of burnishing on corrosion resistance, Mater. Technol. 18 (2003) 155–158, http://dx.doi.org/10.1080/10667857.2003.11753033.
[36] M. Salahshoor, Y.B. Guo, C. Li, Surface integrity and corrosion performance of biomedical magnesium-calcium alloy processed by hybrid dry cutting-finish burnishing, Procedia Manuf. 10 (2017) 467–477, http://dx.doi.org/10.1016/j.promfg.2017.07.030.
[37] Z. Pu, G.L. Song, S. Yang, J.C. Outeiro, O.W. Dillon, D.A. Puleo, I.S. Jawahir, Grain refined and basal textured surface produced by burnishing for improved corrosion performance of AZ31B Mg alloy, Corros. Sci. 57 (2012) 192–201, http://dx.doi.org/10.1016/j.corsci.2011.12.018.
[38] Z. Pu, S. Yang, O.W. Dillon, D.A. Puleo, I.S. Jawahir, Cryogenic burnishing of AZ31B Mg alloy for enhanced corrosion resistance, Magnes. Technol. 2011 (2011) 1–6, http://dx.doi.org/10.1002/9781118062029.ch95.
[39] J. Tang, H.Y. Luo, Y.B. Zhang, Enhancing the surface integrity and corrosion resistance of Ti-6Al-4V titanium alloy through cryogenic burnishing, Int. J. Adv. Manuf. Technol. 88 (2017) 2785–2793, http://dx.doi.org/10.1007/s00170-016-9000-y.
[40] W. Brostow, K. Czechowski, W. Polowski, P. Rusek, D. Tobola, I. Wronska, Slide diamond burnishing of tool steels with adhesive coatings and diffusion layers, Mater. Res. Innov. 17 (2013) 269–277, http://dx.doi.org/10.1179/1433075X12Y.0000000060.
[41] H. Gutiérrez Pulido, R. De la Vara Salazar, Análisis y diseño de experimentos, 2nd ed., McGRAW-HILL/INTERAMERICANA, México, D.F., 2008.
[42] ISO 4287, Geometrical Product Specifications (GPS) – Surface Texture: Profile Method Terms, 1st ed., (1997).
[43] P.H. Gutiérrez, S.R. De la Vara, Análisis y diseño de experimentos, McGraw Hill, México, 2004.
[44] V.F. Lvovich, Impedance Spectroscopy: Applications to Electrochemical and Dielectric Phenomena, John Wiley & Sons, Inc., Hoboken, New Jersey, 2012, http://dx.doi.org/10.1002/9781118164075.
[45] A. Márquez-Herrera, J.L. Fernandez-Muñoz, M. Zapata-Torres, M. Melendez-Lira, P. Cruz-Alcantar, Fe2B coating on ASTM A-36 steel surfaces and its evaluation of hardness and corrosion resistance, Surf. Coat. Technol. 254 (2014) 433–439, http://dx.doi.org/10.1016/j.surfcoat.2014.07.001.
[46] A. Merkys, A. Vaitkus, J. Butkus, M. Okulič-Kazarinas, V. Kairys, S. Gražulis, COD::CIF::parser: an error-correcting CIF parser for the Perl language, J. Appl. Crystallogr. 49 (2016) 292–301, http://dx.doi.org/10.1107/S1600576715022396.
[47] J. Rodríguez-Carvajal, Recent advances in magnetic structure determination by neutron powder diffraction, Phys. B Condens. Matter 192 (1993) 55–69, http://dx.doi.org/10.1016/0921-4526(93)90108-I.